

Efficiency Enhancement of InP Nanowire Solar Cells by Surface Cleaning

Yingchao Cui,^{*,†} Jia Wang,[†] Sebastien R. Plissard,^{†,§} Alessandro Cavalli,[†] Thuy T. T. Vu,[†] Rene P. J. van Veldhoven,[†] Lu Gao,[†] Mike Trainor,[‡] Marcel A. Verheijen,^{†,‡} Jos E. M. Haverkort,[†] and Erik P. A. M. Bakkers^{*,†,§}

[†]COBRA Research Institute, Eindhoven University of Technology, P.O. Box 513, 5600 MB, Eindhoven, The Netherlands

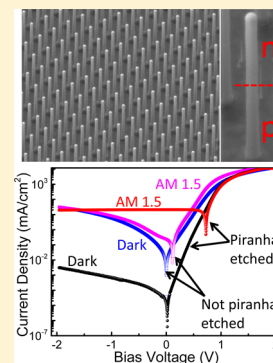
[‡]Philips Innovation Services, High Tech Campus 11, 5656 AE, Eindhoven, The Netherlands

[§]Kavli Institute of Nanoscience, Delft University of Technology, 2600 GA, Delft, The Netherlands

Supporting Information

ABSTRACT: We demonstrate an efficiency enhancement of an InP nanowire (NW) axial p–n junction solar cell by cleaning the NW surface. NW arrays were grown with *in situ* HCl etching on an InP substrate patterned by nanoimprint lithography, and the NWs surfaces were cleaned after growth by piranha etching. We find that the postgrowth piranha etching is critical for obtaining a good solar cell performance. With this procedure, a high diode rectification factor of 10^7 is obtained at ± 1 V. The resulting NW solar cell exhibits an open-circuit voltage (V_{oc}) of 0.73 V, a short-circuit current density (J_{sc}) of 21 mA/cm², and a fill factor (FF) of 0.73 at 1 sun. This yields a power conversion efficiency of up to 11.1% at 1 sun and 10.3% at 12 suns.

KEYWORDS: Nanowires, solar cell, indium phosphide, surface recombination



Semiconductor nanowires (NWs) recently gained increasing attention for photovoltaic applications because of their ability to further improve the balance between solar cell efficiency and device cost.^{1–4} It has been shown that light absorption can be enhanced by using NWs, even at a relative low material volume fraction.^{5,6} As an example, an InP NW array with 2 μm length is predicted to absorb more than 90% of the light above the InP bandgap by optimizing the NW shape and array geometry.^{6,7} Along the same line, it has been reported recently that a single vertically standing GaAs NW features an enhancement of the optical absorption cross section by a factor of 15 compared to the geometrical cross section.⁸ In addition, light absorption in Si NWs can be managed by their cross-sectional shape.^{9,10} One of the most important advantages of a NW is that it allows stacking different materials without the usual severe requirements on lattice matching.¹¹ NW tandem solar cells can be grown by stacking different axial p–n junctions with optimized bandgap on top of each other.^{12,13} An additional advantage for photovoltaic applications is that NWs can be grown on a cheap substrate, for example, group III–V NWs have been successfully grown on Si and Ge.^{14,15} In this study we focus on the optimization of single axial junction NW solar cells.

InP NWs are a good candidate for high-efficiency solar cells,^{16,17} since InP has a very low surface recombination velocity.¹⁸ One important problem for axial NW solar cells is the unintentional radial growth on the NW sidewall, which is

expected to introduce both short circuit shunting paths and nonradiative recombination centers at the NW surface. Although it has been demonstrated that most of this radial growth can be eliminated by *in situ* HCl etching during growth,¹⁹ we recently observed strong unintentional carbon incorporation in a very thin layer at the NW sidewall, even with *in situ* HCl etching.²⁰ In addition, peculiar irregularities are observed on the {111} facets of p-InP NWs grown with HCl.²¹ These irregularities are caused by the presence of sets of stacking faults and are thus expected to be strong trapping centers for minority carriers. Our approach is to perform both *in situ* etching during growth with HCl to prevent the unintentional sidewall growth and, in addition, to perform a postgrowth etching step using a piranha solution to further clean the NW sidewall.

For device fabrication, first a 200 nm p⁺-InGaAs layer (Zn-doped $1.2 \times 10^{19} \text{ cm}^{-3}$) is grown on the backside of a Zn-doped (111)B InP substrate to ensure a p-type ohmic back contact at low annealing temperature ($T < 250 \text{ }^\circ\text{C}$). Subsequently, an array of 136 nm diameter Au particles with 513 nm spacing is prepared using nanoimprint lithography²² on the front side of the substrate. Nanoimprint lithography enables

Received: May 3, 2013

Revised: July 15, 2013

to fabricate uniform NW arrays at wafer scale with low cost and is important to ensure the uniformity and reproducibility of the NW growth. The NWs are subsequently grown in an Aixtron CCS MOVPE system using trimethylindium (TMI) and phosphine (PH_3) at 450°C via the vapor–liquid–solid growth mechanism. HCl is introduced at a 2.83×10^{-5} molar fraction to reduce radial growth.¹⁹ Diethylzinc (DEZn) and H_2S are used as p-type and n-type dopants. The total growth time is 19 min, resulting in a NW length of $2.3 \mu\text{m}$ with the p–n junction located at the middle part of the NWs. Figure 1a,b shows the

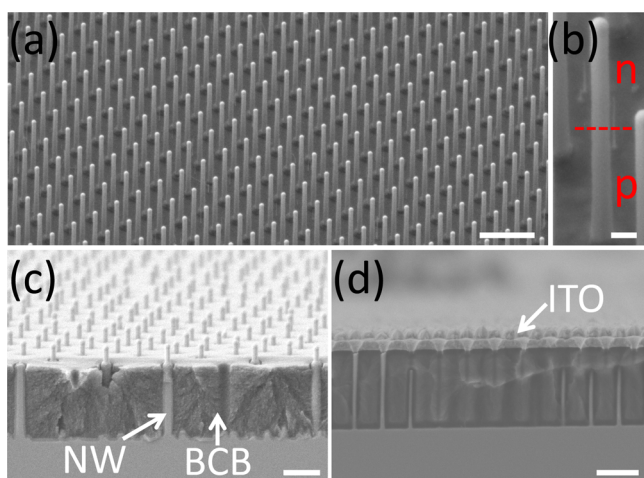


Figure 1. (a) SEM image of the as grown InP NWs tilted by 30° and (b) is the zoom-in image of a single InP NW with a p–n junction. (c) SEM image after BCB planarization and SiO_2 wet etching to expose the tips of the NWs. (d) SEM image after sputtering of the ITO front contact. The scale bar is $1 \mu\text{m}$ for (a, c, d) and 100 nm for (b).

uniformity in both diameter and length of the as-grown InP NWs. Except for the bottom part of the NWs, no apparent lateral growth is observed due to the *in situ* etching with HCl.

After growth, the NWs are etched with a piranha solution to clean the NWs sidewalls. Samples have been prepared with different piranha etching times (0–30 s in steps of 5 s). The etching rate is ~ 0.5 and $\sim 0.3 \text{ nm/s}$ for p-type and n-type InP NW,²⁵ respectively. After etching, the NWs are immediately capped with a 40 nm SiO_2 shell to improve the adhesion between the NWs and the benzocyclobutene (BCB, Dow Chemical) isolation and planarization layer. At the same time SiO_2 is expected to additionally passivate the NW surface.²⁴ The SiO_2 on the NW tips is etched away by buffered HF for making the top contact, as shown in Figure 1c. Ti/Pt/Au is used to form a back contact to the substrate, and 300 nm indium–tin–oxide (ITO) is deposited as the front contact. Finally, the samples are patterned into $500 \mu\text{m} \times 500 \mu\text{m}$ area solar cell devices. A cross section of the final device is shown in Figure 1d, where some wires are missing due to the imperfect cleaving.

The photovoltaic properties of the cells are obtained by measuring the current density–voltage (J – V) characteristics both in the dark and under 1 sun illumination (AM 1.5) with a calibrated setup.²⁸ Figure 2a shows the J – V characteristics of our best solar cell with 25 s piranha etching. Under 1 sun illumination, the solar cell exhibits an open-circuit voltage (V_{oc}) of 0.73 V , a short-circuit current density (J_{sc}) of 21 mA/cm^2 , and a fill factor (FF) of 0.73 , resulting in an overall power conversion efficiency of 11.1% . The high efficiency of the solar

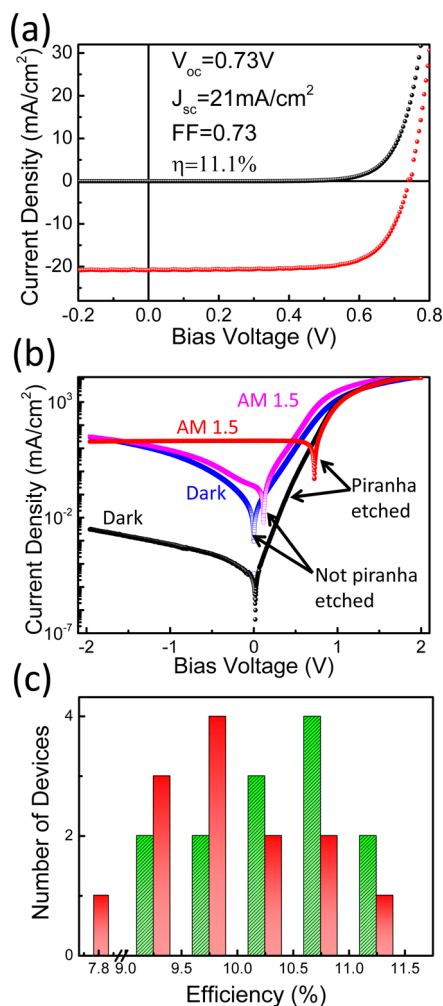


Figure 2. (a) J – V curve of the best nanowire solar cell in the dark and under 1 sun illumination. The NW sidewall was piranha etched for 25 s for this cell. (b) Log J – V characteristics of the best solar cell in the dark (black) and at 1 sun (red). For comparison, we also show the J – V curve without piranha etching in the dark (blue) and at 1 sun illumination (pink). (c) Efficiency distribution of the measured 26 solar cells: the green (slashed) and red columns are from the same sample etched for 25 and 30 s, respectively.

cell is attributed to the low surface recombination velocity of $\text{InP}^{25,26}$ and to the NW sidewall cleaning by both *in situ* etching and postgrowth etching. As compared to the recently reported 13.8% efficiency InP NW axial solar cell with 177 nm diameter NWs,¹⁶ our devices are built from much thinner NWs, which have a 75 nm diameter after sidewall etching. We emphasize that the light absorption in our thin NWs cell could thus be further optimized, e.g., by increasing the NW diameter and using tapered NWs.⁶ We assessed the effect of piranha etching on the device performance in more detail, as shown in Figure 2b. The reverse bias leakage current in the dark is decreased by 3 orders of magnitude by the piranha etching to an extremely low value of $7.5 \times 10^{-4} \text{ mA/cm}^2$ at -1 V bias voltage, corresponding to $\sim 1 \text{ pA}$ per NW. The rectification ratio at $\pm 1 \text{ V}$ simultaneously increases from 10^2 to 10^7 , and the ideality factor (n) improves from 3.17 to 2.12 . The ideality factor $n \geq 2$ indicates that recombination in the space charge region or at the mid-band-gap states dominates our solar cell system. Since NWs have a large aspect ratio and are grown at a relatively low temperature (450°C), surface states and carbon atoms are the

most probable reasons for this value of the ideality factor. In total, we have measured 26 solar cell devices from two different samples, which were fabricated separately and piranha etched for 25 and 30 s, respectively. Figure 2c shows the measured power conversion efficiencies, which vary between 9.2% and 11.1%, except for 1 cell with $\eta < 8\%$ due to local damage to the sample before device fabrication. This shows that, by using nanoimprint lithography, the NW geometry and quality are uniform and reproducible throughout the samples.

To evaluate the surface cleaning effect, we characterized the solar cell properties with different piranha etching times. Figure 3a shows that both V_{oc} and J_{sc} are very low without piranha

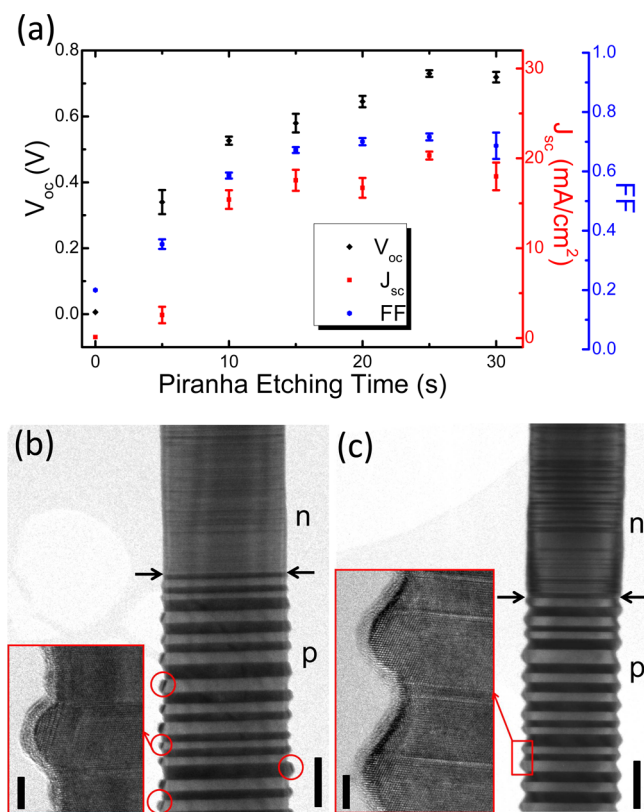


Figure 3. (a) Measured V_{oc} , J_{sc} , and FF for the nanowire solar cell versus the piranha etching time. (b) and (c) are bright-field TEM images of the p–n junction region and high-resolution TEM images of the p-type region InP before and after 25 s piranha etching, respectively. The scale bar is 50 nm for (b) and (c) and 5 nm for the insets of (b) and (c). The arrows indicate the positions of the junctions.

etching, which is attributed to the shunting paths along the NW sidewall introduced by unintentional sidewall growth. As we increase the piranha etching time to 20 s, both V_{oc} and FF increase dramatically. Further increasing the etching time decreases V_{oc} and J_{sc} slightly because the NW diameter is further decreased which also decreases the light absorption in the NW array. In our case the optimum piranha etching time for obtaining the highest power efficiency is 25 s.

In order to investigate the sidewall morphology before and after piranha etching, a transmission electron microscopy (TEM) study was performed on transferred, randomly distributed NWs on a carbon film. The TEM images show that the n-doped region of unetched NWs is wurtzite with only a few stacking faults and vertical side facets. The p-doped

region has the zincblende crystal structure with twin boundaries perpendicular to the growth direction. The side facets are inclined to the growth direction and are irregular in shape. The contrast reversal in the outer part of the nanowire in the bright-field TEM image (see the red circles in Figure 3b) reflects the presence of stacking faults that are inclined to the growth direction (see the HRTEM inset in Figure 3b). These twin planes are the result of imperfect radial growth. According to Wallentin et al., this is related to the presence of HCl during InP growth and can be tuned with the DEZn dopant concentration.²¹ Figure 3c shows that piranha etching is capable to remove the defective outer part of the nanowires, resulting in defect-free, rounded-off {111} and {100} side facets. In addition, our previous photoluminescence (PL) study shows that piranha etching removes the carbon contamination in the unintentionally grown sidewall, which serves as a nonradiative recombination center which deteriorates V_{oc} .²⁰

To investigate the effect of piranha etching and the passivation with a SiO₂ shell on the optical properties, room temperature photoluminescence (PL) lifetime measurements were performed on as-grown NWs, piranha etched NWs, and piranha etched NWs capped with SiO₂ (see the Supporting Information). In this study, pure p-InP and n-InP NWs were grown using the same growth parameters and etching procedures as for the nanowire solar cell. Before piranha etching and without a SiO₂ shell, the PL lifetime of individual p-InP NWs is below the instrumental resolution of ~0.1 ns. The lifetime is improved to 0.18 ns with only piranha etching and further improved to 0.3 ns with piranha etching and additional SiO₂ capping. Similarly, the PL lifetime of the n-InP NWs increases from 0.18 to 0.46 ns, after piranha etching and SiO₂ capping. This is attributed to the elimination of the peculiar irregularities on the sidewalls of the p-InP NWs, the elimination of the carbon impurities in the unintentional grown NW sidewalls, and also to the SiO₂ passivation, which improves and keeps the PL lifetime.²² Presently, the PL lifetimes, in both p-doped and n-doped InP NWs, are not long enough to allow for a ~1 μ m minority carrier diffusion length. However, a terahertz conductivity study recently demonstrated that even with a low PL lifetime of 30 ps a relatively long photoconductivity lifetime of >1 ns is still possible due to charge separation at ZB/WZ crystal phase junctions,¹⁶ which could partly explain the relatively good solar cell performance of our NW solar cell.

The contact between the ITO and the n-InP NWs shows ohmic behavior even using a low annealing temperature ($T < 250$ °C). We performed transmission line measurements (TLM), which show a $2.5 \times 10^{-3} \Omega \text{ cm}^2$ contact resistance between the ITO contacts and a n-InP substrate and a $5.3 \times 10^{-4} \Omega \text{ cm}^2$ contact resistance to the p-InP substrate (see the Supporting Information). These TLM measurements suggest that the series resistance introduced by the contacts is only ~3 Ω per solar cell device ($500 \mu\text{m} \times 500 \mu\text{m}$). The slope of the J – V curve close to V_{oc} in Figure 2a, however, indicates that the series resistance is still a limiting factor. By using a linear fit to the log J – V curve, the estimated series resistance (R_s) is 62 Ω and 84 Ω for a device with and without piranha etching. Moreover, the series resistance decreases to 32 Ω (see the Supporting Information) for devices with a 500 nm shorter p-doped section, implying that R_s mainly originates from twins in the zincblende p-type doped section of the NW solar cells.²⁷

In order to investigate the solar cell performance under concentrated light, we carried out J – V characterization up to an equivalent of 12 suns illumination. As shown in Figure 4, the

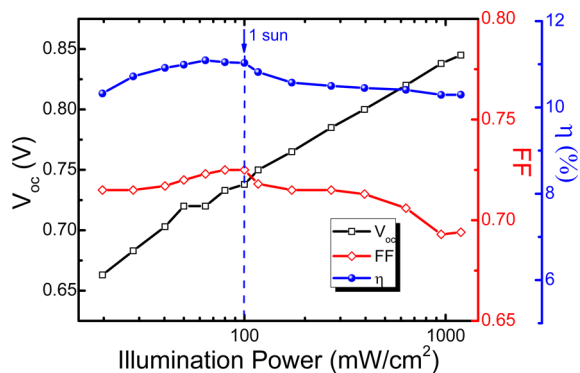


Figure 4. Performance of our highest efficiency nanowire solar cell under concentrated illumination, showing an almost constant efficiency up to 12 suns.

V_{oc} increases logarithmically to 0.845 V when the illumination is increased up to 12 suns, which is expected since $V_{oc} = kT/q \ln(J_{sc}/J_0 + 1)$. Even at 12 suns, only a small decrease in efficiency is observed, from 11.1% to 10.3%. The fill factor only drops 3% because of the series resistance, which is mainly from the p-InP segment, as discussed above. Finally, the cells have been stored in ambient air for more than 3 months, and no efficiency degeneration has been observed.

In conclusion, a high-efficiency axial InP NW array solar cell is demonstrated by improving the surface quality of the NW by postgrowth sidewall etching. By the sidewall etching, we removed (i) short-circuit current paths along the NW sidewall, (ii) the radially grown part of the nanowires containing sets of stacking faults, particularly on the {111} side facets, and (iii) carbon that was unintentionally incorporated in the radially grown NW volume. Our NW solar cells show extremely low dark leakage current (~ 1 pA/NW) and high rectifying behavior (10^7 at ± 1 V). We finally obtain a high V_{oc} of 0.73 V and a high fill factor of 0.73, resulting in a solar cell efficiency of 11.1% at 1 sun. Finally, our solar cell shows an almost constant efficiency up to 12 suns.

■ ASSOCIATED CONTENT

Supporting Information

Detailed procedures of the device fabrication, data of the contact resistances, and photoluminescence lifetime measurements. This material is available free of charge via the Internet at <http://pubs.acs.org>.

■ AUTHOR INFORMATION

Corresponding Author

*E-mail: y.cui@tue.nl (Y.C.); e.p.a.m.bakkers@tue.nl (E.P.A.M.B.).

Notes

The authors declare no competing financial interest.

■ ACKNOWLEDGMENTS

We acknowledge the long-term energy and innovation program EOS-LT, which is funded by Agentschap NL, as well as the Cobra research school funded by NWO. We also acknowledge the technical support from the NanoLab@TU/e cleanroom. We thank Prof. R. E. I. Schropp for providing access to a calibrated solar simulator at ECN.

■ ABBREVIATIONS

NW, nanowire; BCB, benzocyclobutene.

■ REFERENCES

- Garnett, E. C.; Brongersma, M. L.; Cui, Y.; McGehee, M. D. *Ann. Rev. Mater. Res.* **2011**, *41* (1), 269–295.
- Tian, B.; Kempa, T. J.; Lieber, C. M. *Chem. Soc. Rev.* **2009**, *38* (1), 16–24.
- Tian, B. Z.; Zheng, X. L.; Kempa, T. J.; Fang, Y.; Yu, N. F.; Yu, G. H.; Huang, J. L.; Lieber, C. M. *Nature* **2007**, *449* (7164), 885–U8.
- Hochbaum, A. I.; Yang, P. D. *Chem. Rev.* **2010**, *110* (1), 527–546.
- Kelzenberg, M. D.; Boettcher, S. W.; Petykiewicz, J. A.; Turner-Evans, D. B.; Putnam, M. C.; Warren, E. L.; Spurgeon, J. M.; Briggs, R. M.; Lewis, N. S.; Atwater, H. A. *Nat. Mater.* **2010**, *9* (3), 239–244.
- Diedenhofen, S. L.; Janssen, O. T. A.; Grzela, G.; Bakkers, E. P. A. M.; Rivas, J. G. *ACS Nano* **2011**, *5* (3), 2316–2323.
- Anttu, N.; Xu, H. Q. *J. Nanosci. Nanotechnol.* **2010**, *10* (11), 7183–7187.
- Krogstrup, P.; Jorgensen, H. I.; Heiss, M.; Demichel, O.; Holm, J. V.; Aagesen, M.; Nygard, J.; Fontcuberta i Morral, A. *Nat. Photonics* **2013**, *7* (4), 306–310.
- Kim, S. K.; Day, R. W.; Cahoon, J. F.; Kempa, T. J.; Song, K. D.; Park, H. G.; Lieber, C. M. *Nano Lett.* **2012**, *12* (9), 4971–4976.
- Fan, Z. Y.; Kapadia, R.; Leu, P. W.; Zhang, X. B.; Chueh, Y. L.; Takei, K.; Yu, K.; Jamshidi, A.; Rathore, A. A.; Ruebusch, D. J.; Wu, M.; Javey, A. *Nano Lett.* **2010**, *10* (10), 3823–3827.
- Wallentin, J.; Persson, J. M.; Wagner, J. B.; Samuelson, L.; Deppert, K.; Borgstrom, M. T. *Nano Lett.* **2010**, *10* (3), 974–979.
- Heurlin, M.; Wickert, P.; Falt, S.; Borgstrom, M. T.; Deppert, K.; Samuelson, L.; Magnusson, M. H. *Nano Lett.* **2011**, *11* (5), 2028–2031.
- Borgstrom, M. T.; Wallentin, J.; Heurlin, M.; Falt, S.; Wickert, P.; Leene, J.; Magnusson, M. H.; Deppert, K.; Samuelson, L. *IEEE J. Sel. Top. Quantum Electron.* **2011**, *17* (4), 1050–1061.
- Shin, J. C.; Kim, K. H.; Yu, K. J.; Hu, H.; Yin, L.; Ning, C. Z.; Rogers, J. A.; Zuo, J. M.; Li, X. *Nano Lett.* **2011**, *11* (11), 4831–8.
- Bakkers, E. P. A. M.; van Dam, J. A.; De Franceschi, S.; Kouwenhoven, L. P.; Kaiser, M.; Verheijen, M.; Wondergem, H.; van der Sluis, P. *Nat. Mater.* **2004**, *3* (11), 769–73.
- Wallentin, J.; Anttu, N.; Asoli, D.; Huffman, M.; Aberg, I.; Magnusson, M. H.; Siefer, G.; Fuss-Kailuweit, P.; Dimroth, F.; Witzigmann, B.; Xu, H. Q.; Samuelson, L.; Deppert, K.; Borgstrom, M. T. *Science* **2013**, *339* (6123), 1057–1060.
- Goto, H.; Nosaki, K.; Tomioka, K.; Hara, S.; Hiruma, K.; Motohisa, J.; Fukui, T. *Appl. Phys. Exp.* **2009**, *2*, 035004.
- Joyce, H. J.; Wong-Leung, J.; Yong, C. K.; Docherty, C. J.; Paiman, S.; Gao, Q.; Tan, H. H.; Jagadish, C.; Lloyd-Hughes, J.; Herz, L. M.; Johnston, M. B. *Nano Lett.* **2012**, *12* (10), 5325–30.
- Borgstrom, M. T.; Wallentin, J.; Tragardh, J.; Ramvall, P.; Ek, M.; Wallenberg, L. R.; Samuelson, L.; Deppert, K. *Nano Res.* **2010**, *3* (4), 264–270.
- Vu, T. T.; Zehender, T.; Verheijen, M. A.; Plissard, S. R.; Immink, G. W.; Haverkort, J. E.; Bakkers, E. P. *Nanotechnology* **2013**, *24* (11), 115705.
- Wallentin, J.; Wickert, P.; Ek, M.; Gustafsson, A.; Reine Wallenberg, L.; Magnusson, M. H.; Samuelson, L.; Deppert, K.; Borgstrom, M. T. *Appl. Phys. Lett.* **2011**, *99* (25), 253105.
- Pierret, A.; Hocevar, M.; Diedenhofen, S. L.; Algra, R. E.; Vlieg, E.; Timmering, E. C.; Verschuuren, M. A.; Immink, G. W. G.; Verheijen, M. A.; Bakkers, E. P. A. M. *Nanotechnology* **2010**, *21*, 6.
- van Weert, M. H. M.; Helman, A.; van den Einden, W.; Algra, R. E.; Verheijen, M. A.; Borgstrom, M. T.; Immink, G.; Kelly, J. J.; Kouwenhoven, L. P.; Bakkers, E. P. A. M. *J. Am. Chem. Soc.* **2009**, *131* (13), 4578–4579.
- Chevchenko, S. A.; Reshchikov, M. A.; Fan, Q.; Ni, X.; Moon, Y. T.; Baski, A. A.; Morkoc, H. *J. Appl. Phys.* **2007**, *101*, 11.

(25) Mariani, G.; Scofield, A. C.; Hung, C. H.; Huffaker, D. L. *Nat. Commun.* **2013**, *4*, 1497.

(26) Fukui, T.; Yoshimura, M.; Nakai, E.; Tomioka, K. *Ambio* **2012**, *41*, 119–124.

(27) Dick, K. A.; Thelander, C.; Samuelson, L.; Caroff, P. *Nano Lett.* **2010**, *10* (9), 3494–3499.

(28) The solar simulator is calibrated with a reference cell measured at ECN, The Netherlands.